This is the accepted manuscript made available via CHORUS. The article has been published as:

Scaling of velocity and scalar structure functions in ac electrokinetic turbulence

Wei Zhao and Guiren Wang

Phys. Rev. E **95**, 023111 — Published 22 February 2017

DOI: 10.1103/PhysRevE.95.023111

Scaling of velocity and scalar structure functions in AC electrokinetic turbulence

Wei Zhao[1,2] and Guiren Wang[2,3,*]

[1] Institute of Photonics and Photo-technology, International Scientific and Technological Cooperation Base of Photoelectric Technology and Functional Materials and Application, Northwest University, 229 North Taibai Rd, Xi'an 710069, People's Republic of China

[2] Department of Mechanical Engineering, [3] Biomedical Engineering Program, University of South Carolina, USA.

*Email: guirenwang@sc.edu

Electrokinetic (EK) turbulence or electrohydrodynamic (EHD) turbulence has been recently achieved in different fluids under both AC (Wang et al, Lab on a Chip 14, 1452 – 1458, 2014; Wang et al, Physical Review E, 2016, 93, 013106) and DC electric fields (Varshney et al, Soft Matter 16, DOI: 10.1039/c5sm02316e). Here, through dimensional analysis, new scaling laws of both velocity and electric conductivity structure functions in the forced cascade region of AC EK turbulence can be predicated (similar to Bolgiano-Obukhov scaling law (BO59) in turbulent Rayleigh-Bénard (RB) convection), in either **macroscale** or **microscale flows**. In the forced cascade region, EK force, which relies on the direct cascade of conductivity structures, injects energy directly into a wide spectral region to sustain the flow disturbance. The scaling exponents of the second order velocity and conductivity structures are 2/5 and 4/5 respectively. Accompanied with the new scaling regions, two characteristic small length scales are derived, for both the weak and strong electric body force (EBF) respectively. This theoretical investigation can significantly enhance our understanding on the EK or EHD turbulence while forced by an AC electric field. It can further broaden our understanding on the forced cascade region of forced turbulence and make the manipulation of turbulent cascade process more flexible and controllable.

1. Introduction

In 1941, Kolmogorov [1] established the classic self-similarity law (K41 law) in high Reynolds number (Re) turbulence. In the theory, based on the homogeneous and isotropic hypothesis of turbulence, the p^{th} order streamwise velocity structure function ($\Delta u(l) = u(x+l) - u(x)$) in the inertial subrange, is directly related to the corresponding spatial scale — l as below:

$$S_u^p(l) = \langle \Delta u(l)^p \rangle \tag{1}$$

$$S_u^2(l) = \langle \Delta u(l)^2 \rangle \sim \epsilon_u^{2/3} l^{2/3} \tag{2}$$

where $S_u^2(l)$ is the 2nd order structure function of u, $< >$ indicates ensemble averaging, $\epsilon_u = 2\nu s_{ij} s_{ij}$ is turbulent energy dissipation rate, ν is kinematic viscosity of fluid and s_{ij} is strain-rate tensor respectively [2]. Later, Obukhov (1949) [3] and Corrsin (1951) [4] extended this work to scalar fields and showed that, by passive convection, in the inertial subrange of scalar turbulence, the scalar structure function ($\Delta\varphi(l) = \varphi(x+l) - \varphi(x)$) has:

$$S_\varphi^2(l) = \langle \Delta\varphi(l)^2 \rangle \sim \epsilon_\varphi \epsilon_u^{-1/3} l^{2/3} \tag{3}$$

where $\epsilon_\varphi = 2D_\varphi \langle (d\varphi/dx)^2 \rangle$ is the scalar dissipation rate of φ and D_φ is the diffusivity of the scalar. Then, in 1959, Batchelor [5] extended the scaling theory of scalar turbulence from inertial subrange to viscous-advection subrange for high Schmidt (or Prandtl) number fluids. The slope of scalar (such as concentration) power spectrum in the viscous-advection subrange is -1. All of the three scaling laws are for cascade processes, which are dominated by inertial convection and molecular diffusion (or viscosity). In the same year, Bolgiano [6] and Obukhov [7] advanced the so called Bolgiano-Obukhov scaling law (BO59) in stably stratified atmosphere respectively, as shown below:

$$S_u^2(l) \sim \epsilon_T^{2/5} (\alpha g)^{4/5} l^{6/5} \tag{4a}$$

$$S_T^2(l) \sim \epsilon_T^{4/5} (\alpha g)^{-2/5} l^{2/5} \tag{4b}$$

where T indicates temperature, "α" is the thermal expansion coefficient and "g" is gravity. This law for the first time predicts the scaling behavior in forced cascade region where buoyancy is important. Previously, many efforts have been made to verify BO59 law in Rayleigh-Bénard (RB) turbulent convection. Niemela et al (2000) [8] claimed they experimentally observed the temperature spectrum related to BO59 law in a RB convection. However, due to the single-point measurement that relies on the validity of Taylor Hypothesis, the experimental results still remain debatable. Even after almost five decades, the existence of BO59 law in RB turbulence is still not proved faithfully [9]. Nevertheless, in Raleigh-Taylor (RT) turbulence, the BO59 law and the corresponding Bolgiano scale (l_B) [6] have been both theoretically [10] and numerically [11, 12] discovered.

The investigations on Electro-hydrodynamic (EHD) flow was initialized in 1960s, as reviewed by Saville (1977) [13]. However, the researches on EHD turbulence are much later and the fruits are limited. Davidson and Shaughnessy (1986) [14] introduced a method of generating turbulence by electric body force in a large scale precipitator. This leaded a wide use of EHD turbulence in industry. However, our understanding on the mechanism of EHD turbulence, such as the energy cascade process, is really rare. After nearly 30 years, Kourmatzis and Shrimpton (2012) [15] first numerically investigated the dielectric EHD turbulence analogous to RB turbulence. They focused on the EHD turbulence, but their computational spectra of the flow velocity have slopes around or steeper than -3, implying the flow could still be chaotic, not fully turbulent. The early investigations on EHD turbulence are primarily about large scale flows. Recently, Wang et al [16] discovered turbulent behavior in a electrokinetic (EK) microflow, by measuring velocity and concentration fluctuations[17]. In the investigation, two streams with large initial ratio of electric conductivities were injected into a microchannel by syringe pump. When a strong AC electric field (at 100 kHz) was applied, the flow became highly disordered and spatiotemporally random [16]. Their further investigations showed that under the AC EK forcing, some flow feathers of high Re turbulence, such as -5/3 spectrum, self-similarity of velocity structures and exponential tail of the probability density function of velocity gradient etc, could also be observed [18]. As the AC EK turbulence was generated in a microchannel, the phenomena should be more common and achievable in macroscale EHD flows.

Accompanied with the new founds in the AC EK turbulence, several problems have emerged. For example, when an AC electric field of 100 kHz was applied, it was found that the velocity and concentration fluctuated at a much lower spectral region (less than 2 kHz). Why? What is the cascade process of turbulent energy in the AC EK turbulence?

To make the problems clear, we investigate the AC EK turbulence by comparing it with RB (as well as RT) turbulence. On one hand, the energy cascade process in the micro-EK flow seems to be similar to that of RB flow, by substituting the buoyancy force with an electric body force (even though the buoyancy has a fixed direction, while the electric body force (EBF) is more flexible), as shown in Eq. (5) and FIG. 1. On the other hand, in RB convection, since buoyancy is determined by local fluid temperature (i.e. scalar itself), its influence on flow by energy injection decreases with the reduction of scale rapidly ($\sim l^{4/5}$) [9, 19]. Hence, buoyancy can only affect the large scale velocity structures. While in the EK turbulence, the EBF depends essentially on the electric field intensity and the gradient of conductivity (i.e. gradient of scalar). Thus, the EBF decreases with decreasing l with a smaller scaling exponent (smaller than 4/5 in RB flows), and results in a stronger influence on small-scale velocity structures, as discussed later. Therefore, EK turbulence is apparently different from the turbulent RB convection and is more observable in macroflows at small scales and even microfluidics. Large-scale velocity

fluctuations could be generated by either fluid inertia at high Re flow or by EBF at low Re flow, initially. Followed is the turbulence energy cascades from large to small scales with continuous injection of energy by EBF.

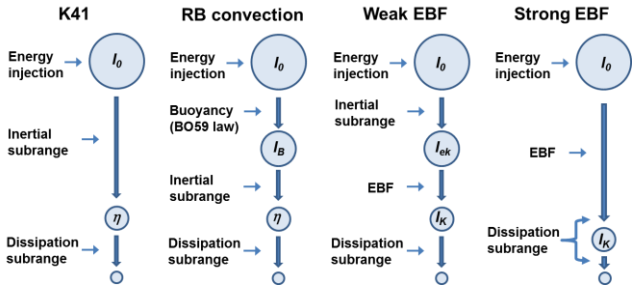

FIG.1 Schematic of energy cascade in K41 model, RB turbulence and EK turbulence with different EBFs. l_B is the Bolgiano scale. η is Kolmogorov scale. l_0 is a characteristic large length scale. For hydrodynamic turbulence, l_0 is normally the integral scale. In RB turbulence, l_0 is either integral scale or geometric scale of the flow cell. In EK turbulence, l_0 is still the characteristic large length scale, while l_{ek} and l_K are two additional characteristic small scales, which will be introduced in details below.

The purpose of the present work is to theoretically study the scaling behavior of the velocity and conductivity structures when the AC EBF dominates energy cascading processes. The EBF of AC electric fields on scale l is derived first. Then, the energy cascade process due to AC EBFs is presented. Later, the scaling laws of both velocity and electric conductivity structures in the EBF dominated subrange are advanced. New characteristic small scales relevant to the new scaling laws are developed in the meanwhile. Since the coupling between velocity and EBF are complicated, necessary hypotheses are required to simplify the model. The validity of the hypotheses is discussed finally.

2. Theory derived from scale based EBF

2.1 Control equations and hypotheses

In EK flows, the fluid can still be assumed to be continuum and incompressible. The conservation equation of momentum is [20]:

$$\rho\frac{D\boldsymbol{u}}{Dt} = -\nabla p + \mu\nabla^2\boldsymbol{u} + F_e \tag{5}$$

where ρ is fluid density, $\boldsymbol{u} = u\vec{\imath} + v\vec{\jmath} + w\vec{k}$ is the instant velocity vector (u, v and w are the velocity in streamwise (x), spanwise (y) and vertical (z) direction respectively as shown in FIG. 2. $\vec{\imath}$, $\vec{\jmath}$ and $\vec{k}$ are the corresponding unit vectors in the directions), μ is dynamic viscosity of the fluid and $D/Dt = \partial/\partial t + \boldsymbol{u}\cdot\nabla$. F_e is EBF which can be expressed as [21]:

$$F_e = \rho_e\boldsymbol{E} - \frac{1}{2}(\boldsymbol{E}\cdot\boldsymbol{E})\nabla\varepsilon \tag{6}$$

$$\rho_e = \nabla\cdot(\varepsilon\boldsymbol{E}) = \nabla\varepsilon\cdot\boldsymbol{E} + \varepsilon\nabla\cdot\boldsymbol{E} \tag{7}$$

where ρ_e is the net charge density, $\boldsymbol{E}$ is the electric field intensity and $\boldsymbol{E} = E_x\vec{\imath} + E_y\vec{\jmath} + E_z\vec{k}$. σ and $\varepsilon = \varepsilon_r\varepsilon_0$ are the electric conductivity and permittivity of the solution respectively. ε_r is the relative permittivity and ε_0 is vacuum permittivity**.**

In this investigation, we require [22]:

$$\tau_{rex} \ll 1/\omega \ll \tau_{mig} \ll \tau_{diff} \tag{8}$$

where $\omega = 2\pi f_f$ is the angular frequency of AC electric field, f_f is the corresponding AC frequency, $\tau_{rex} = \varepsilon/\sigma$ is the charge relaxation time, $\tau_{mig} = l/b|\boldsymbol{E}|$ is the migration time scale of ions in electric field and $\tau_{diff} = l^2/D_\sigma$ is the diffusion time scale of ions respectively. l is the considered length scale, b is the mobility of ions in solution, $|\boldsymbol{E}|$ indicates the magnitude of electric intensity, D_σ is the effective diffusivity of ions respectively. Under the scheme of Eq. (8), the conservation equation of charge can be described as [20-22]:

$$\partial\rho_e/\partial t + \nabla\cdot(\sigma\boldsymbol{E}) + \nabla\cdot(\rho_e\boldsymbol{u}) = 0 \tag{9}$$

In Eq. (9), $\nabla\cdot(\sigma\boldsymbol{E})$ represents the generation of ρ_e by local conductivity and electric field intensity, and $\nabla\cdot(\rho_e\boldsymbol{u})$ is the convective transport of ρ_e. As have been discussed by Ramos et al[21], compared to $\nabla\cdot(\sigma\boldsymbol{E})$, the convection term $\nabla\cdot(\rho_e\boldsymbol{u})$ has a much smaller influence on the variation of net charge and can be neglected (also see discussion 5.1 for details). Therefore, Eq. (9) can be simplified as:

$$\frac{\partial\rho_e}{\partial t} + \nabla\cdot(\sigma\boldsymbol{E}) = 0 \tag{10}$$

It can be seen the variation of ρ_e is determined by the distribution of local σ and $\boldsymbol{E}$. Note, $\boldsymbol{E}$ is also affected by the distribution of σ. Hence, σ plays an important role in EK flows. Under the condition of Eq. (8), the conservation equation of σ can be described as [20, 22]:

$$\frac{D\sigma}{Dt} = D_\sigma\nabla^2\sigma \tag{11}$$

where $D_\sigma = (D_+b_- + D_-b_+)/(b_+ + b_-)$, D_+ and D_- are the diffusivities of positive and negative ions respectively, and b_+ and b_- are the mobilities of positive and negative ions respectively. The conservation equation of σ is a typical convection-diffusion equation, just as the temperature in RB (or RT) turbulence. This is why we can study σ by analogous to T in RB turbulence.

To completely investigate the turbulent flow caused by EBF, normally, one needs to solve Eq. (5), (10) and (11) in wide spatial and temporal scale ranges simultaneously. If electrothermal effect is also important, the transport equation of temperature is additionally required. The complex coupling relations among velocity, conductivity, electric field intensity and even temperature makes the theoretical investigation on

the AC EK turbulence to be extremely difficult in practice. Meanwhile, to solve the wide scale range of spatial - temporal vector and scalar quantities in the coupling nonlinear equations requires huge computational capacity and high-efficiency algorithms. So far, to the best of our knowledge, only Kourmatzis and Shrimpton (2012) preliminarily investigated 3D EHD turbulence with significant simplifications (such as neglecting the fluctuation of electric field) on the models. Nevertheless, their results about EHD turbulence are still debatable and more relevant to chaotic flow[23]. Recently, the investigation of Wang et al (2014)[16] implies the electric field intensity can have less coupling with the velocity and electric conductivity (indicated by the fluorescent dye concentration) fields, since the applied frequency of AC electric field can be much higher than the spectral regions of velocity and dye concentration. This can significantly simplify the complex flow field and make the theoretical analysis available.

In this investigation, we consider a simplified AC EK flow that related to the scheme of Wang et al [16-18] as an example, but not limited to it, to show how the AC EK turbulence can be generated. Two flows with the **same** initial velocity, viscosity, temperature, electric permittivity etc, but **different** electric conductivities, are injected into a channel. The mixture is convected downstream and disturbed by the AC electric field. This flow field is similar to that of RT turbulence with convection, where two streams with different temperatures are injected into an adiabatic channel and evolve downstream under the influence of buoyancy. Under the disturbance from a sufficiently large EBF, an equilibrium state of EK turbulence with approximately 1D AC electric field is expected to be achieved, if the following three hypotheses can be satisfied.

H1. This hypothesis is generally consistent with that in Obukhov-Corrsin law [3, 4]. There exists an equilibrium region of electric conductivity in the flow field, when the fluids are highly mixed (but not on molecular level). In the region,

- **(H1.1)** *The electric conductivity is homogeneous without mean conductivity gradient*. This means $\bar{\sigma}$, $\overline{\sigma'^2}$ and all the higher order statistical quantities of σ are constant in the equilibrium region. The bar indicates temporal averaging;
- **(H1.2)** *The structural function of electric conductivity is locally isotropic*, then the 3D structural function can be statistically simplified to 1D; [3, 4]
- **(H1.3)** *The variance of electric conductivity cascades directly from large to small scale*. The large scale σ structures are generated by the mixed fluids with different electric conductivities. Then, by cascading, the variance of σ is transported from the large to small scales. Thus, the cascade of σ is a direct and passive process. Although σ could change with temperature which can be primarily affected by electrothermal effect, in this investigation, the temperature variation due to electrothermal effect is ignored. This is because, the electrothermal effect comes mainly from the Joule heating, of which the heating power is $\sim\sigma|\boldsymbol{E}|^2$ [21]. Due to **H1.1** and **H1.4** (see below), the heating in the equilibrium region is homogeneous (dominated by $\bar{\sigma}$ which is constant) with negligible variation of temperature. Therefore, the electric conductivity variation cannot be significantly affected by temperature variation;
- **(H1.4)** *The electric conductivity fluctuation, relative to its mean value, is small*. This is to say, $\langle\sigma'^2\rangle^{1/2}/\langle\sigma\rangle \ll 1$, where $\sigma' = \sigma - \langle\sigma\rangle$. Note, in the equilibrium region, $\langle\sigma\rangle = \bar{\sigma}$.

H2. The electric field can be approximated as a 1D model. As schemed in FIG. 2, an external electric field is applied in *y*-direction. Due to **H1.1**, **H1.2** and **H1.4**, when the distribution of σ is locally homogeneous, isotropic with small variation, the local electric field intensity has $E_x \sim E_z \ll E_y$ (see section 5.3 for details). Therefore, **H2** can be approximately satisfied and the local $\boldsymbol{E}$ in the 1D model is mainly in *y*-direction. Note, only the electric field is assumed to be 1D. The velocity and conductivity fields are still 3D. This is similar to the case in RB turbulence where gravity field can be approximately 1D, but the velocity field is highly 3D.

H3. The frequency of applied external AC electric fields is much higher than the response frequency of the flow. In other words, the frequency of the applied external AC electric field is so high that the flow cannot respond immediately to the instantaneous AC electric field. From the spectral space, the spectral bandwidth of velocity and σ must be far from that of the AC electric field. **H3** is an important hypothesis to simplify the AC EK flows. It is based on the experimental observations by Wang et al (2014)[16], where they applied an AC electric field with forcing frequency $f_f = 100$ kHz, but a wide and continuous frequency ranges of both velocity and dye concentration were discovered below 2 kHz which is much smaller than f_f. This indicates, σ and the flow velocity induced by EBF could change much slower than the external AC electric field which is on the time scale of $t_f = 1/f_f$. Therefore, these quantities have negligible cross correlations with the applied high frequency AC signal. Our analysis on the flow under AC electric field can be significantly simplified.

2.2 AC EBF on scale *l*

Based on the hypothesis **H3**, it is reasonable to assume, on the time scale of t_f, the pattern of σ structures is frozen, since the variation of σ is on the time scale of $t_s = 1/f_\sigma \gg t_f$ (where f_σ is the characteristic frequency of σ fluctuation, $f_\sigma \ll f_f$). Hence, the amplitude of $\boldsymbol{E}$, i.e. $E_m(x,y,z,t_s)$ which is determined by the σ distribution and the applied electric field, varies at f_σ as shown in FIG. 3a. Since $f_\sigma \ll f_f$, the instant electric field intensity with the amplitude $E_m(x,y,z,t_s)$ oscillates quasi-periodically at f_f, as shown in FIG. 3b, which is a zoom-in view of the region highlighted by dashed lines in FIG. 3a. Therefore, relying on **H2**, $\boldsymbol{E}$ can be approximately described as:

$$\boldsymbol{E} = E_y(x,y,z,t)\vec{j} = E(x,y,z,t)\vec{j} = E_m(x,y,z,t_s)e^{i\omega t}\vec{j} \tag{12}$$

Here, we use E instead of E_y for short. Substitute $\boldsymbol{E}$ (Eq. (12)) and ρ_e (Eq. (7)) into Eq. (10), for the 1D model, we have:

$$\frac{\partial}{\partial t}\frac{\partial(\varepsilon E)}{\partial y} + \frac{\partial(\sigma E)}{\partial y} = 0 \tag{13}$$

It should be noted, although ε in the two streams is initially the same, it still has variations downstream due to the temperature fluctuation generated by both electrothermal effect and heat transfer. However, based on **H1.3**, the temperature variation (due to σ variation) is trivial, the influence of temperature on ε is weak and the related ε variation is negligible too. Here, we keep it in Eq. (13) for generality.

The first term of Eq. (13) can be derived as:

$$\frac{\partial}{\partial y}\frac{\partial(\varepsilon E)}{\partial t} = \frac{\partial}{\partial y}\left[i\omega\varepsilon E + E\frac{\partial\varepsilon}{\partial t} + \varepsilon e^{i\omega t}\frac{\partial E_m(x,y,z,t_s)}{\partial t}\right] \tag{14}$$

Because the time scales of both $E_m(x,y,z,t_s)$ and ε are determined by the relatively slow varying flow on the order of t_s (compared to the fast varying AC signal on t_f), their instant variation on the smaller time scale t_f could be approximated as:

$$\frac{\partial E_m(x,y,z,t_s)}{\partial t} \sim \frac{E_{m,rms}}{t_s} \tag{15a}$$

$$\frac{\partial\varepsilon}{\partial t} = \frac{\partial\varepsilon}{\partial T}\frac{\partial T}{\partial t} \sim \frac{\partial\varepsilon}{\partial T}\frac{T_{rms}}{t_s} \tag{15b}$$

where the subscript "rms" indicates temporal root-mean-square values. As a result of **H1.1**, $E_{m,rms}$ is constant in the equilibrium region. Therefore, Eq. (14) becomes:

$$\frac{\partial}{\partial y}\frac{\partial(\varepsilon E)}{\partial t} \approx \frac{\partial}{\partial y}\left(i\omega\varepsilon E + E\frac{\partial\varepsilon}{\partial T}\frac{T_{rms}}{t_s} + \varepsilon e^{i\omega t}\frac{E_{m,rms}}{t_s}\right) \tag{16}$$

In the investigation, if the fluid is water, $T_{rms} \ll 100$ K. As $(1/\varepsilon)(\partial\varepsilon/\partial T) = -0.004$ per degree [21, 24], it can be seen:

$$\frac{\partial}{\partial y}\frac{\partial(\varepsilon E)}{\partial t} \approx \frac{\partial}{\partial y}\varepsilon\left(i\omega E - 0.004ET_{rms}f_\sigma + e^{i\omega t}E_{m,rms}f_\sigma\right) \tag{17}$$

When the fluctuation of σ relative to its mean value is small, as restricted by **H1.4**, $E_{m,rms}$ is also negligibly small compared to the value of $E_m(x,y,z,t_s)$ for $\forall\, t_s, x, y$ and z. Therefore, $\omega E_m(x,y,z,t_s) \gg E_{m,rms}f_\sigma$ and the third term on the right side of Eq. (17) can be neglected. In the meanwhile, since $\omega \gg 0.004T_{rms}f_\sigma$, the second term which represents the influence of temperature on ε can also be neglected. Then, Eq. (17) can be approximated to:

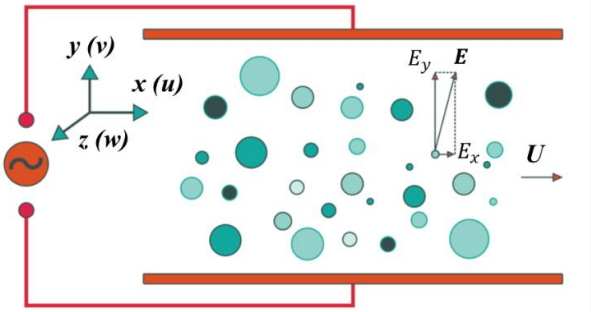

FIG. 2 Schematic of the 1D model of electric field that proposed in **H2**, where "1D" means $E_x \sim E_z \ll E_y$. The circles with different size and colors indicate electric conductivity structures with different scales and electric conductivities.

$$\frac{\partial}{\partial y}\frac{\partial(\varepsilon E)}{\partial t} \approx \frac{\partial}{\partial y}(i\omega\varepsilon E) \tag{18}$$

Combing Eq. (13) and (18), we have:

$$\frac{\partial i\omega\varepsilon E}{\partial y} + \frac{\partial\sigma E}{\partial y} = \frac{\partial\sigma^* E}{\partial y} = 0 \tag{19}$$

where $\sigma^* = \sigma + i\omega\varepsilon$ is the complex electric conductivity. Thus, for 1D case, even though in a turbulent flow, the complex Ohmic law is approximately satisfied, as below:

$$\sigma^* E = J^*(x,z,t) \tag{20}$$

where J^* is the complex electric current density along y-direction but independent of y. In fact, J^* is independent with x and z, as introduced later.

Since from **H3**, $t_s \gg t_f$, i.e. the flow cannot immediately respond to the high frequency of the AC electric field, the AC EBF in Eq. (6) can be rewritten as [21]:

$$F_{e,AC} = \frac{1}{2}\mathrm{Real}\left(\rho_e \cdot \tilde{E} - \frac{1}{2}E^2\nabla\varepsilon\right) \tag{21}$$

where "~" means complex conjugate. $F_{e,AC}$ is actually a temporal averaging of instant AC EBF on time scale t_s. Based on the 1D electric field model, we have:

$$F_{e,AC} = \frac{1}{2}\mathrm{Real}\left[\left(\frac{\partial\varepsilon}{\partial y}E + \varepsilon\frac{\partial E}{\partial y}\right)\tilde{E}\right]\vec{j} - \frac{1}{4}\mathrm{Real}(E^2)\nabla\varepsilon$$

$$= \frac{1}{4}\frac{\partial\varepsilon E_{md}^2}{\partial y}\vec{j} + \frac{1}{4}E_{md}^2\frac{\partial\varepsilon}{\partial y}\vec{j} - \frac{1}{4}\mathrm{Real}(E^2)\nabla\varepsilon \tag{22}$$

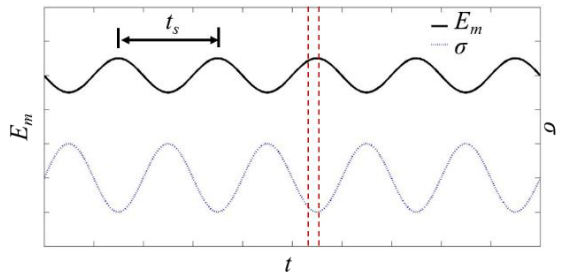

(a)

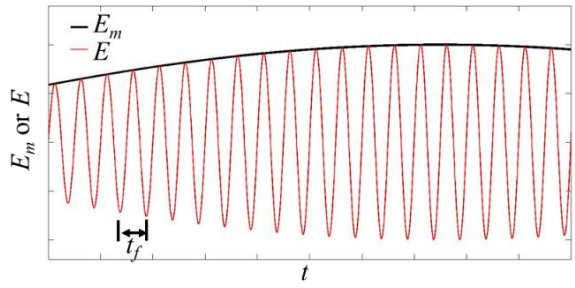

(b)

FIG. 3 Relation of the electric field intensity with a time scale t_s in a 1D model. (a) In the model, E_m varies with local σ in a qualitatively inverse relation under time scale t_s. (b) The instant E varies in a short time period as highlighted by the dashed line of (a), as an example. On the time scale t_f, the variation of E_m is very small, since $f_\sigma \ll f_f$. In the time region of (b), E varies under f_f with a slightly varying E_m.

where $E_{md}^2 = E\tilde{E}$. Each term of $F_{e,AC}$ can be estimated as below:

$$\begin{cases} \text{Real}(E^2)\nabla\varepsilon \le E_{md}^2\nabla\varepsilon \sim E_{md}^2\nabla T\frac{\partial\varepsilon}{\partial T} \sim E_{md}^2\frac{\partial\varepsilon}{\partial T}\frac{T_{rms}}{l} \ll \frac{0.4\varepsilon E_{md}^2}{l} \\ E_{md}^2\frac{\partial\varepsilon}{\partial y} \ll \frac{0.4\varepsilon E_{md}^2}{l} \\ \frac{\partial\varepsilon E_{md}^2}{\partial y} \sim \frac{\varepsilon E_{md}^2}{l} \end{cases} \tag{23}$$

Therefore, the last two terms of Eq. (22) are significantly smaller than the first one and can be ignored. The AC EBF can be approximated to a *y*-direction force as below:

$$F_{e,AC} = \frac{1}{4}\frac{\partial\varepsilon E_{md}^2}{\partial y}\vec{J} \tag{24}$$

For σ structures on scale l, the averaged EBF is:

$$F_{e,l} = \langle F_{e,AC}\rangle_l = \frac{1}{l}\int_y^{y+l} F_{e,AC}\,dy = \frac{1}{4l}\varepsilon E_{md}^2\Big|_y^{y+l} \tag{25}$$

where $\langle * \rangle_l$ indicates the spatial averaging on scale l in *y*-direction. By substituting Eq. (20) into (25), $F_{e,l}$ becomes:

$$F_{e,l} = \frac{\varepsilon}{4l}E_{md}^2\Big|_y^{y+l} = \frac{\varepsilon}{4l}E\tilde{E}\Big|_y^{y+l} = \frac{\varepsilon}{4l}\frac{J^*\widetilde{J^*}}{\sigma^*\widetilde{\sigma^*}}\Big|_y^{y+l} = \frac{\varepsilon}{4l}\frac{|J^*|^2}{|\sigma^*|^2}\Big|_y^{y+l} \tag{26}$$

To estimate the influence of J^*, new quantities that evaluate the equivalent influence of σ and σ^* on scale l are introduced as below:

$$\begin{cases} \sigma_l^* = 1/\langle 1/\sigma^*\rangle_l \\ \sigma_l = 1/\langle 1/\sigma\rangle_l \end{cases} \tag{27}$$

σ_l and σ_l^* can be considered as the reciprocal of electric resistivity averaged on scale l. The electric field intensity on scale l is defined as:

$$E_l = \langle E\rangle_l \tag{28}$$

Based on the quantities defined in Eq. (27) and (28), we have the following conservative relation:

$$\sigma^* E = \sigma_l^* E_l = \sigma_w^* E_w = J^* \tag{29}$$

where "w" is the channel width. By defining σ_l and σ_l^*, the complex J^* is directly related with the scale-based conductivity and electric field intensity. Also, the small scale quantities are directly related with large scale quantities. From **H1.1**, σ_w^* is approximately constant. $E_w = V^*/w = E_{amp}e^{i\omega t}$ is also independent of *x*, *y* and *z*, where V^* is the externally applied complex voltage on the two electrodes shown in FIG. 2 and E_{amp} is the amplitude of electric field across the solution. Therefore, from Eq. (29), it can be predicted J^* is statistically uniform at each moment for $\forall x$ and z positions, and $|J^*|^2(t) = E_w\widetilde{E_w}\sigma_w^*\widetilde{\sigma_w^*}$.

By applying linear approximation of σ variation on scale l, we can find:

$$\begin{aligned} \frac{1}{|\sigma^*|^2}\Big|_y^{y+l} &= \frac{1}{\sigma^2(y+l)+\omega^2\varepsilon^2} - \frac{1}{\sigma^2(y)+\omega^2\varepsilon^2} = \frac{1}{\left[\sigma_{m,l}+\frac{1}{2}\Delta\sigma(l)\right]^2+\omega^2\varepsilon^2} - \\ \frac{1}{\left[\sigma_{m,l}-\frac{1}{2}\Delta\sigma(l)\right]^2+\omega^2\varepsilon^2} &= -2\frac{1}{\sigma_{m,l}^2}\frac{\Delta\sigma(l)/\sigma_{m,l}}{\left[1+\frac{1\Delta\sigma^2(l)}{4\ \sigma_{m,l}^2}+\frac{\omega^2\varepsilon^2}{\sigma_{m,l}^2}\right]^2-\frac{\Delta\sigma^2(l)}{\sigma_{m,l}^2}} \end{aligned} \tag{30}$$

Let $\theta_l = \Delta\sigma(l)/\sigma_{m,l}$, $\beta = \omega\varepsilon/\sigma$, $\beta_l = \omega\varepsilon/\sigma_{m,l}$, $\sigma_{m,l} = [\sigma(y+l)+\sigma(y)]/2$, Eq. (30) becomes:

$$\frac{1}{|\sigma^*|^2}\Big|_y^{y+l} = -2\frac{1}{\sigma_{m,l}^2}\frac{\theta_l}{\left[1+\frac{1}{4}\theta_l^2+\beta_l^2\right]^2-\theta_l^2} \tag{31}$$

Furthermore, as $\tau_{rex} \ll 1/\omega$ is satisfied globally, it is certainly $\beta_l \ll 1$. Also, when the two streams have equal flow rates, initially $|\theta_l| \in [0,2]$. After highly mixed, as restricted by **H1.4**, $|\theta_l| \ll 1$. In the range of θ_l above, both binominal expansion and Taylor expansion are applicable for Eq. (31), and the expansion result is:

$$\frac{\theta_l}{\left[1+\frac{1}{4}\theta_l^2+\beta_l^2\right]^2-\theta_l^2} \sim \theta_l\left(1+\frac{1}{2}\theta_l^2-2\beta_l^2\right) \tag{32}$$

By substituting Eq. (31), (32) and (33) into Eq. (26), we have:

$$F_{e,l}(x,y,z,t) = -\frac{\varepsilon}{2l}\frac{E_w\widetilde{E_w}\sigma_w^*\widetilde{\sigma_w^*}}{\sigma_{m,l}^2}\theta_l\left(1+\frac{1}{2}\theta_l^2-2\beta_l^2\right) \tag{33}$$

Furthermore, since there is no initial difference of ε between the two streams and local temperature variation on ε is negligible, based on $\tau_{rex} \ll 1/\omega$ from Eq. (8), $\varepsilon\omega$ has negligible variation in the flow field compared to the variation

of σ. Therefore, we have,

$$\Delta\sigma^*(l) = \sigma^*(y+l) - \sigma^*(y) \approx \Delta\sigma(l) = \sigma(y+l) - \sigma(y) \tag{34}$$

From Eq. (27) and (34), again assume σ has linear variation on scale l, then it can be seen:

$$\sigma_l^* = \frac{1}{\langle\frac{1}{\sigma^*}\rangle_l} = \frac{1}{\frac{1}{l}\int_0^l \frac{1}{\sigma^*}dy} = \frac{l}{\int_0^l \frac{1}{\sigma^*(y)+\frac{y'}{l}[\sigma^*(y+l)-\sigma^*(y)]}dy'} =$$

$$\frac{\sigma^*(y+l)-\sigma^*(y)}{\ln\frac{\sigma^*(y+l)}{\sigma^*(y)}} \approx \frac{\Delta\sigma(l)}{\ln\left[\frac{\sigma_{m,l}^*+\Delta\sigma(l)/2}{\sigma_{m,l}^*-\Delta\sigma(l)/2}\right]} \tag{35}$$

where $\sigma_{m,l}^* = [\sigma^*(y+l) + \sigma^*(y)]/2$. The denominator of Eq. (35) can be expanded as:

$$\begin{aligned}
&\ln\left[\frac{\sigma_{m,l}^*+\Delta\sigma(l)/2}{\sigma_{m,l}^*-\Delta\sigma(l)/2}\right] \\
&= \ln\left[\sigma_{m,l}^*+\Delta\sigma(l)/2\right] - \ln\left[\sigma_{m,l}^*-\Delta\sigma(l)/2\right] \\
&= \ln\left[\sigma_{m,l}(1+i\beta_l+\theta_l/2)\right] - \ln\left[\sigma_{m,l}(1+i\beta_l-\theta_l/2)\right] = \\
&= \ln[1+\theta_l/2(1+i\beta_l)] - \ln[1-\theta_l/2(1+i\beta_l)]
\end{aligned} \tag{36}$$

Since $|\theta_l| \ll 1$, by applying Taylor expansion to the order of $O(\theta_l)$, we have:

$$\ln\left[\frac{\sigma_{m,l}^*+\Delta\sigma(l)/2}{\sigma_{m,l}^*-\Delta\sigma(l)/2}\right] \approx \frac{\theta_l}{1+i\beta_l} \tag{37}$$

and then Eq. (35) becomes:

$$\sigma_l^* \approx \Delta\sigma(l)(1+i\beta_l)/\theta_l \tag{38}$$

As $\Delta\sigma(l)/\theta_l = \sigma_{m,l}$ and $\sigma_{m,l}(1+i\beta_l) = \sigma_{m,l}^*$, it is easily seen:

$$\sigma_l^* \approx \sigma_{m,l}^* \tag{39a}$$

Similar results can also be applied for σ_l, which is:

$$\sigma_l \approx \sigma_{m,l} \tag{39b}$$

Therefore, as a result of **H1**, we can summarize a series of approximations:

$$\begin{cases} \sigma_{m,l} \approx \sigma_{m,w} \approx \sigma_l \approx \sigma_w \approx \langle\sigma\rangle_w \\ \sigma_{m,l}^* \approx \sigma_{m,w}^* \approx \sigma_l^* \approx \sigma_w^* \\ \sigma_{m,l_l}^* \approx \sigma_{m,w}^* \approx \widetilde{\sigma_l^*} \approx \widetilde{\sigma_w^*} \end{cases} \tag{40}$$

Based on the Eq. (40), it is easily found $\beta_l \approx \beta_w \approx \omega\varepsilon/\langle\sigma\rangle_w$ and $\sigma_w^*\widetilde{\sigma_w^*} = \sigma_{m,w}^*\widetilde{\sigma_{m,w}^*} = \sigma_{m,w}^2 + \omega^2\varepsilon^2$. Note that $E_w = E_{amp}e^{i\omega t}$, while neglecting $O(\theta_l^3)$, Eq. (33) becomes:

$$F_{e,l}(x,y,z,t_s) = -\frac{\varepsilon E_{amp}^2\theta_l}{2l}(1-\beta_w^2) \tag{41}$$

Eq. (41) shows the AC EBF is determined by the conductivity structures on scale l through θ_l which is a low frequency component below f_σ. This clearly indicates, through $F_{e,l}$, the work of AC EBF can be transfer to kinetic energy and injected into the flow at a much lower frequency region than f_f.

Therefore, the energy cascade of velocity in EK turbulence is not a purely direct cascade process, but coupled with the continuous energy injection by EBF. Relatively, the conductivity cascade is a purely direct process. The energy cascade relies on the conductivity cascade, which controls the EBF and feedbacks to affect the conductivity cascade process.

2.3 Scaling law in EBF dominated cascade region (EBF dominated subrange)

When the scalar structure functions have self-similarities as:

$$S_\sigma^1(l) = \langle|\Delta\sigma(l)|\rangle \sim \langle|\Delta\sigma(l_0)|\rangle(l/l_0)^{\delta_{\sigma,1}} \tag{43a}$$

we can get a dimensionless scaling relation as below:

$$\langle|\theta_l|\rangle \sim \langle|\theta_{l_0}|\rangle l^{*\delta_{\sigma,1}} \tag{43b}$$

where l_0 is a reference large scale, $0 < l^* = l/l_0 \le 1$, and $\delta_{\sigma,p}$ is the scaling exponents of p^{th} order structure function of σ. In the equilibrium region of electric conductivity, $F_{e,l}$ and the induced velocity structures on scale l are plotted in FIG. 4. From the dimensional analysis and Eq. (41), the structure function of the EBF induced velocity ($v^2 \sim |F_{e,l}|l/\rho$) [20] on scale l can be described as:

$$S_v^2(l) = \langle[v(x,y+l) - v(x,y)]^2\rangle \sim \left\langle\left[\sqrt{\frac{|F_{e,l}|l}{\rho}} - \left(-\sqrt{\frac{|F_{e,l}|l}{\rho}}\right)\right]^2\right\rangle = 4\langle|F_{e,l}|\rangle l/\rho \sim \Lambda\, l^{*\delta_{\sigma,1}}/\rho \sim l^{*\delta_{\sigma,1}} \tag{44}$$

where $\Lambda = 2\langle|\theta_{l_0}|\rangle\varepsilon E_{amp}^2(1-\beta_w^2)$ is a large-scale nominal function. Note, for the equilibrium region of conductivity, $\langle[v(x,y+l)-v(x,y)]^2\rangle \sim \langle[v(x+l,y)-v(x,y)]^2\rangle$, as schemed by FIG. 4. As $S_v^2(l) \sim l^{*\delta_{v,2}}$, we have:

$$\delta_{v,2} = \delta_{\sigma,1} \text{ or } \delta_{\varepsilon,1} \tag{45}$$

Compared to the well-known energy cascade in the inertial subrange of turbulence, which is dominated by a constant turbulent energy dissipation, the cascade process of turbulent energy in the EBF dominated subrange relies on the cascade of electric conductivity structures. Therefore, in the EBF dominated subrange, the transport of electric conductivity plays a key role in the cascade process.

In the AC EK turbulence, the transport of electric conductivity is not simply a passive process. On one hand, the flow is driven by EBF due to electric conductivity structures and local electric field intensity. On the other hand, the electric conductivity structures are passively cascaded by the velocity structures in the flow simultaneously. This is similar to the temperature transport in RB turbulence [9], where, temperature is convected under the velocity field induced by temperature difference. Furthermore, both σ in the AC EK turbulence and T in RB turbulence satisfy the same type of convection-diffusion equation, i.e. $D\varphi/Dt = \kappa\nabla^2\varphi$. The difference is only the value of diffusivity κ. Therefore, there is no difference between the transport of electric conductivity in the AC EK turbulence and that of temperature in RB turbulent convection. The conservation law for the flux of temperature structure can be equivalently used for that of σ, under the Obukhov-Corrsin picture [9].

In the AC EK turbulence, the flux of σ structure, i.e.

$\langle\Delta\sigma(l)^2\rangle\langle\Delta v(l)^2\rangle^{1/2}/l$, is uniquely determined by the electric conductivity dissipation rate which is constant in the aforementioned equilibrium region. This leads to $l^{2.5\delta_{\sigma,1}}\sim l$, and then:

$$\delta_{v,2} = \delta_{\sigma,1} = 2/5 \text{ and } \delta_{\sigma,2} = 4/5 \quad (46)$$

Therefore, the scaling behavior of the second order moments of velocity structures and conductivity structures in EK dominated scale region can be expressed as:

$$S_v^2(l)\sim l^{2/5} \quad (47a)$$

$$S_\sigma^2(l)\sim l^{4/5} \quad (47b)$$

From Eq. (44) and (46), we further get:

$$\langle|F_{e,l}|\rangle\sim\Lambda l_0^{-2/5} l^{-3/5} \quad (48a)$$

$$Gr_{e,l}\sim\langle|F_{e,l}|\rangle l^3/\rho\nu^2 \sim \Lambda l_0^{-2/5} l^{12/5}/\rho\nu^2 \quad (48b)$$

$$Ra_{e,l} = Gr_{e,l}Sc\sim\Lambda l_0^{-2/5}\, l^{12/5}/\rho\nu D_\sigma \quad (48c)$$

where $Gr_{e,l}$ and $Ra_{e,l}$ are the scale based electric Grashof number and electric Rayleigh number respectively; $Sc = \nu/D_\sigma$ is the Schmidt number of ions in liquids.

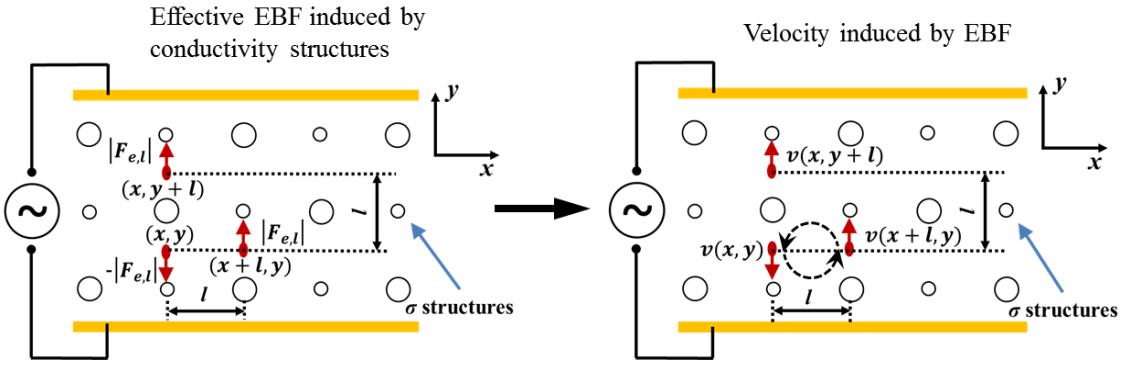

FIG. 4 Relation between AC EBF at scale l and its induced flow velocities. At an arbitrary moment, because of the different conductivity gradient on y-direction, AC EBFs can be generated in opposite directions as shown in the left figure. The induced flows in opposite directions because of the AC EBFs will form vortex structures when the turnover time of a vortex is short enough. Hence, the velocity structures in both x- and y-directions are statistically equivalent.

3. Theory from dimensional analysis

The scaling behavior can also be achieved by the following analysis. Superficially, the EBF is dominated by ρ, $\nabla\varepsilon$ and $\boldsymbol{E}$, as shown in Eq. (5) and (6). It is reasonable to consider that the cascade process is also determined by the density of fluids, electric field intensity and electric permittivity (or the complex counterpart). However, in the AC EK turbulence, as $\tau_{rex} \ll 1/\omega$ and the variation of ε is neglected, the variation of complex permittivity is not determined by ε, but σ/ω which has the same dimension as ε. Therefore, the dimensional influence of electric permittivity should be replaced by σ/ω. As ω is a constant, the cascade process is actually attributed to the evolution of σ.

In the equilibrium region of the AC EK turbulence, since the influence of temperature on σ is neglected and no additional electrolyte is introduced, the flow field becomes a close system of σ, compared with the open system for flow velocity. The variance of σ (and the related magnitude of complex electric permittivity) cascades from large to small scales. The cascade process of the complex electric permittivity determines how much external work can be applied on the fluids. Therefore, it is very important on the generation of AC EK turbulence. The cascade process of complex electric permittivity can be analyzed by analogous to that of temperature in RT turbulence.

In RT turbulence, where BO59 law is also theoretically and numerically applicable [10-12], the temperature cascade is determined by the dissipation rate of temperature. While in the AC EK turbulence, the cascade process of complex electric permittivity can also be evaluated by a single parameter — the scalar dissipation rate ($\epsilon_\varepsilon\sim D_\sigma\langle[(\partial\varepsilon/\partial x)^2 + (\partial\sigma/\partial x)^2/\omega^2]\rangle$ of the complex electric permittivity.

Therefore, the second order momentum of velocity structures in the EBF dominated subrange of the AC EK turbulence should have the following dimensional relations:

$$S_v^2(l)\sim\epsilon_\varepsilon^a E_{amp}^b \rho^c l^d \quad (49)$$

By proper dimensional analysis, we have:

$$S_v^2(l)\sim\epsilon_\varepsilon^{2/5} E_{amp}^{8/5}\rho^{-4/5} l^{2/5} \quad (50)$$

From Eq. (8) where $\tau_{rex} \ll 1/\omega$, it is found $\partial(\sigma/\omega)/\partial x \gg \partial\varepsilon/\partial x$ (the latter is approximately zero). This results in:

$$\epsilon_\varepsilon\sim\epsilon_\sigma/\omega^2 \quad (51)$$

where $\epsilon_\sigma = \langle D_\sigma(\partial\sigma/\partial x)^2\rangle$. Then, Eq. (50) has another more relevant format:

$$S_v^2(l)\sim\epsilon_\sigma^{2/5} E_{amp}^{8/5}\omega^{-4/5}\rho^{-4/5} l^{2/5} \quad (52)$$

Similarly, the scaling of σ structures can be easily derived as:

$$S_\sigma^2(l) \sim \epsilon_\sigma^{4/5} E_{amp}^{-4/5} \omega^{2/5} \rho^{2/5} l^{4/5} \quad (53)$$

Apparently, the results of dimensional analysis are consistent with what we found in Eq. (39a).

4. The universal expressions of characteristic length scales

By comparing Eq. (44) and (52), and arbitrarily defining:

$$G\left(\langle|\theta_{l_0}|\rangle; \beta_w\right) \sim \left[2\langle|\theta_{l_0}|\rangle(1-\beta_w^2)\right]^{5/2} \quad (54)$$

which is a dimensionless function that evaluates the influence of large scale σ structures and the forcing frequency, we find the large scale l_0 can be estimated as:

$$l_0 \sim G\rho^{-1/2}\varepsilon^{5/2} E_{amp} \epsilon_\sigma^{-1} \omega^2 \quad (55)$$

l_0 predicts the upper bound of the EBF dominated subrange. In practice, if the EBF dominated subrange is confined within a channel, the actual l_0 cannot be larger than the geometric scale of flow field in the channel. In this case, people should use the geometric scale of the channel rather than the l_0 calculated from Eq. (55), as the upper bound scale of the EBF dominated subrange. From Eq. (48a), it can be seen, the spatially averaged EBF on scale l, i.e. $\langle|F_{e,l}|\rangle$, increases with decreasing l, while the total EBF on scale l conductivity structures, i.e. $\langle|F_{e,l}|\rangle l$, increases with l, as $\langle|F_{e,l}|\rangle l \sim l^{2/5}$. This indicates, although the total EBF also decreases with decreasing l, the force is more effective at smaller scales, compared to the buoyancy in RB convections ($\sim l^{4/5}$). This difference results in a different cascade process in the EBF dominated subrange from that in the RB convection.

(1) Weak EK turbulence: If the EBF effect is weak, the inertial subrange still exists. The length scale on which the EBF dominant region and inertial subrange are connected can be found by balancing Eq. (2) and (52), which is:

$$l_{ek} \sim \epsilon_\sigma^{3/2} \epsilon_v^{-5/2} E_{amp}^6 \omega^{-3} \rho^{-3} \quad (56)$$

l_{ek} and l_0 have the following relation:

$$l_{ek}/l_0 \sim G^{-1}\omega^{-5}\left(E_{amp}^2/\rho\varepsilon\right)^{5/2}(\epsilon_\sigma/\epsilon_v)^{5/2} \quad (57)$$

Besides, since AC EBF increases with the decreasing l rapidly, when the Schmidt number of ions in electrolytes is much larger than unity, the influence of the EBF becomes significant at a very small length scale l_K. On l_K, the velocity fluctuations generated by the EBF are directly dissipated by viscous dissipation. l_K can be defined and determined by equalizing the turn-over time of small scale eddies (estimated by the electric inertial velocity) to the viscous diffusion time, as:

$$l_K/\sqrt{S_v^2(l_K)} = l_K^2/\nu \quad (58)$$

By substituting Eq. (52) into (58), we have:

$$l_K/\sqrt{\epsilon_\sigma^{2/5} E_{amp}^{8/5} \omega^{-4/5} \rho^{-4/5} l_k^{2/5}} \sim l_K^2/\nu \quad (59)$$

Then,

$$l_K \sim \epsilon_\sigma^{-1/6} E_{amp}^{-2/3} \omega^{1/3} \rho^{1/3} \nu^{5/6} \quad (60)$$

In this case, normally the free flow velocity is large and the electric field intensity is small. The cascade process of kinetic energy can be divided into four subregions, as shown in FIG.1. (1) First, the kinetic energy of flow will be injected from the large scale l_0 accompanied with the injection of σ variance. (2) Then, the inertial subranges for both energy and conductivity cascades involve till scale l_{ek}. The formation of inertial subrange is due to both direct energy cascade from large scale velocity fluctuations and the inverse cascade from EBF dominant subregion. (3) In the EBF dominant subregion, i.e. $l_{ek} \gg l \gg l_K$, since the AC EBF increases with the decreasing l, EBF becomes stronger and stronger. The energy cascade process is effectively manipulated by the AC EBF based on the cascading of σ variance. The scaling exponents of velocity and electric conductivity structures have been predicted by Eq. (47a) and (b). (4) Beyond the inertial subrange, at smaller scales below l_K, the viscous dissipation becomes dominated.

It can be seen, the energy cascade in the weak EK turbulence is **different** to that in the RB convection.

(2) Strong EK turbulence: When the EBF is sufficiently strong, l_{ek} approaches l_0 and l_K is significantly small. In such a case, the cascading process of kinetic energy has only three subranges, as shown in FIG.1. (1) In the first subrange, at the low wavenumber part, i.e. less than $2\pi/l_0$, the conductivity variance is injected into the flow region from large scale. (2) Then, since the EBF is very strong, the EBF dominated subrange can sustain to the wavenumber $2\pi/l_K$, and no inertial subrange is present. In this subrange, both velocity and scalar structures are expressed by the relations in Eq. (47a) and (b). (3) Beyond $2\pi/l_K$, the kinetic energy injected by the AC EBF is directly dissipated by viscous dissipation and the dissipation subrange is expected.

The relations between l_K and l_0 can be easily setup as below. Since in the present scheme of AC EK turbulence, the difference of σ is initially injected into the flow field and convected downstream, the input rate of conductivity variance can be described by $\langle\sigma'^2\rangle/\tau$, where $\tau = l_0/\sqrt{S_v^2(l_0)}$ is a characteristic convection time scale in the equilibrium region. The input conductivity variance must be dissipated in the region when equilibrium state is reached. Hence, the conductivity dissipation rate can be expressed as:

$$\epsilon_\sigma = \sqrt{S_v^2(l_0)}\langle\sigma'^2\rangle/l_0 \sim E_{amp}\omega^{-1/2}\rho^{-1/2} l_0^{-1} \langle\sigma'^2\rangle^{5/4} \quad (61)$$

This expression indicates, when the large scale velocity stirring is enhanced, more σ variance could be injected into the region in unit time, since the initial conductivities of the two streams are the same and constant. If the input rate of the conductivity variance is increased, but l_0 is still constant, it indicates the averaged ϵ_σ is increased. Furthermore, if ϵ_σ does not change while the input rate of conductivity variance is increased, a larger region is required for the conductivity variance to be dissipated.

By substituting Eq. (61) into (60), we have:

$$l_K \sim Gr_e^{-5/12}\beta_w^{5/12} l_0 = Ra_e^{-5/12} Sc^{5/12}\beta_w^{5/12} l_0 \quad (62)$$

where $Gr_e = \varepsilon l_0^2 E_{amp}^2 \langle \sigma'^2 \rangle^{1/2}/\rho\nu^2\langle\sigma\rangle_w$ is the electric Grashof number on large scale, $Ra_e = Gr_e Sc$ is the electric Rayleigh number. From Eq. (62), it is obtained:

$$l_K/l_0 \sim Gr_e^{-5/12}\beta_w^{5/12} = Ra_e^{-5/12} Sc^{5/12}\beta_w^{5/12} \quad (63)$$

This implies, to achieve a wider EBF dominated subrange, larger Gr_e and Ra_e, or smaller β_w and Sc are required. Note, $Sc \gg 1$ is required for the theory. In a confined scheme, when the EBF is sufficiently strong, the equilibrium region could fulfill the entire channel and $l_0 \approx w$. In this case, Gr_e and Ra_e can be evaluated by the corresponding nominal value, i.e. $Gr_{en} = \varepsilon w^2 E_{amp}^2 \langle \sigma'^2 \rangle^{1/2}/\rho\nu^2\langle\sigma\rangle_w$ and $Ra_{en} = \varepsilon w^2 E_{amp}^2 \langle \sigma'^2 \rangle^{1/2}/\rho\nu D_\sigma\langle\sigma\rangle_w$, respectively.

In the strong EK turbulence, l_K is normally very small. But it cannot be infinitesimal and should be restricted by several characteristic length scales, which are: (a) $l_{rex,mig} = \varepsilon b|\boldsymbol{E}|/\sigma$ is the length scale on which the electric migration time scale is comparable to the charge relaxation time; (b) $l_{rex,diff} = \sqrt{\varepsilon D_\sigma/\sigma} = \delta\sqrt{\beta/2Sc}$ is another small length scale on which the ion diffusion time scale is comparable to the charge relaxation time. $\delta = \sqrt{2\nu/\omega}$ is the thickness of acoustic boundary layer [25]; and (c) $l_{Bat} = l_K/\sqrt{Sc}$ is an alternative Batchelor's scale (analogous to the conventional Batchelor's scale [5]).

From Eq. (8), we know our theoretical model in this investigation requires the length scales to be larger than both $l_{rex,mig}$ and $l_{rex,diff}$. Meanwhile, at scales smaller than l_{Bat}, there will be no apparent conductivity structures to sustain EBF and the EBF dominated subrange disappears. However, since *Sc* is much larger than unity, l_K can never be smaller than l_{Bat}. Thus, the restriction from l_{Bat} can be ignored. The theoretical model in this investigation only requires l_K to be equal to or larger than $l_{rex,mig}$ and $l_{rex,diff}$. This can be achieved by increasing the mean conductivity and conductivity variance, selecting optimal AC frequency, applying stronger $\boldsymbol{E}$ and adopting the electrolytes in solution with larger *Sc* (larger *Sc* will cause smaller $l_{rex,diff}$ and make the condition $l_{rex,diff} < l_K$ more achievable).

5. Discussion

The feature that EBF can sustain to small scales makes the AC EK turbulence achievable not only in macroflows, but also in microflows. It can significantly enhance the transport of scalar variance from large to small scales, and as a result, rapid fluid mixing can be achieved. Compared to the previous investigations on EK chaotic flows based on EK flow instability [26-30], the mixing through EK turbulence can be much faster.

It should be noted, although the investigation is based on the simplified model introduced above, it is not restricted to this flow system. The model is applicable for all the AC EK flows that satisfy the three hypotheses. After the analysis above, we revisit the aforementioned pre-requirements and hypotheses.

5.1 The validity of $\tau_{rex} \ll 1/\omega \ll \tau_{mig} \ll \tau_{diff}$ in Eq. (8)

In practice, to change the conductivity of a solution, one normally uses buffer solutions. The ions of buffer solution can be Na^+, Ca^{2+} and Cl^- etc, whose electric mobilities are around 5×10^{-8} m^2/Vs and the effective diffusivities are on the order of 10^{-9} m^2/s, respectively [22]. For a typical AC EK flow, e.g. the one investigated by Wang et al (2014)[16], where $E_{amp} = 10^5$ V/m and $\varepsilon = 10^{-9}$ F/m, at an averaged conductivity $\sigma = 2500$ μS/cm, the time scales corresponding to a 1 μm conductivity structure are: $\tau_{rex} = 4 \times 10^{-9}$ s, $\tau_{mig} = 2 \times 10^{-4}$ s and $\tau_{diff} = 10^{-3}$ s respectively. Clearly, on this length scale or above, $\tau_{rex} \ll 1/\omega \ll \tau_{mig} \ll \tau_{diff}$ can be easily achieved. Meanwhile, if the characteristic length scale of conductivity is increased, τ_{diff} will increase faster than τ_{mig}. Hence, the difference among τ_{rex}, τ_{mig} and τ_{diff} can be further increased and Eq. (8) could be more easily achieved.

Furthermore, the validity of the simplification in Eq. (9). i.e. neglecting $\nabla\cdot(\rho_e\boldsymbol{u})$, can also be proved. There are generally three reasons. First, the generation of net charge is on the order of τ_{rex}, while the convective time scale is on the order of l/U. Only when $U \gg l/\tau_{rex}$, the influence of the convection on the variation of net charge becomes important. For a typical condition considered above, τ_{rex} could be on the order of 10^{-9} s. For a small scale (say $l = 1$ μm), U should be on the order of 10^3 m/s for the convection term to generate significant influence. This is extremely difficult in an EK flow, no matter for macro-or microflows. Second, one can decrease l to achieve smaller l/τ_{rex}, but l cannot be infinitesimal. Otherwise no conductivity gradient can exist on that small scale. Third, as restricted by Eq. (8) and **H3**, the convective time scale $l/U \gg 1/\omega \gg \tau_{rex}$. Therefore, the convection has smaller influence on the variation of net charges, which are primarily and instantly induced by the local conductivity gradient and electric field intensity. We can confidently neglect the convection term from Eq. (9).

5.2 The validity of H1

H1 is an important and commonly used hypothesis in scalar turbulence[3, 4]. In the AC EK turbulence, the aforementioned equilibrium state can be realized by at least two methods. First, it can be put into practice by electrically disturbing, when the Gr_e, Ra_e or the equivalent electric Reynolds number etc are sufficiently high. The other way is by turbulent mixing in a pre-existed high Reynolds number turbulence. In this method, when fluids with different conductivities have been mixed, the required equilibrium state could be formed, if a strong AC electric field is applied.

The AC EBF would be able to manipulate the energy and conductivity cascade as predicted in Eq. (47).

Moreover, as shown in many experiments, the isotropy of velocity and scalar fields is not strictly required to realize either K41 law [31] or Obukhov-Corrsin law [32, 33]. Therefore, in our model, the requirement of local isotropy (i.e. **H1.2**) could be slightly relaxed. Meanwhile, the requirement of small conductivity fluctuations can be easily satisfied, since a mixedness of more than 90% can often be achieved in micro- [34] and macromixers [35], no matter by hydrodynamic or EK methods. Therefore, **H1** is valid and achievable in practice.

5.3 The validity of H2

Although the external AC electric field is in *y*-direction only, the E_x and E_z components that caused by the nonuniform distribution of induced charge are not exactly zero, but negligibly small. The 1D hypothesis of electric field can be supported from two facts.

First, in the considered model, we require the conductivity field to have relatively weak fluctuations, i.e. $\theta_l \ll 1, \forall l$. Since the external electric field is in *y*-direction, in *x* and z-directions, the spatially averaged electric field intensity are zero, i.e. $\langle E_x \rangle = \langle E_z \rangle = 0$ at any time. However, in *y*-direction, the spatially averaged electric field intensity is $\langle E_y \rangle = E_{amp}\cos(\omega t)$. E_{amp} is normally much larger than zero. In the meanwhile, due to the homogeneous and isotropic distribution of electric conductivity (**H1.1** and **H1.2**), the fluctuations of E_x, E_y and E_z that replies on σ' are all on the order of $E_{m,rms}$. Therefore, $E_y = \langle E_y \rangle + E_{m,rms} \gg E_x = \langle E_x \rangle + E_{m,rms} \sim E_z = \langle E_z \rangle + E_{m,rms}$.

Second, since the external electric field is in *y*-direction, E_x and E_z are induced by net charge ρ_e accumulation around electric conductivity structures due to $\nabla\sigma$. As indicated in Fig. 5, to have large E_x (or E_z), the ions should be significantly separated and moved through electric migration by E_y. This requires the averaged displacement of ions in *y*-direction must be on the order of the characteristic length scale of electric conductivity structures, or even larger. However, as restricted by $1/\omega \ll \tau_{mig}$, our theory stands in the scale range $l \gg l_{AC,mig} = b|\boldsymbol{E}|/\omega$. This is equivalent to say, in our model, we only consider l_K (the lower bound of EBF dominated subrange) to be much larger than $l_{AC,mig}$. During forcing by AC electric field in *y*-direction, the displacement of ions in *y*-direction is on the order of $l_{AC,mig}$. The induced internal electric field $E_{y,in} \sim \rho_e / l_{AC,mig}^2 \ll E_y$. In the meanwhile, the distance of induced ions in *x* and *z* directions are larger or equal to l_K. Therefore, $E_x \sim E_z \leq \rho_e / l_K^2$. Since $l_{AC,mig} \ll l_K$, we have $E_y \gg E_{y,in} \gg E_x \; or \; E_z$.

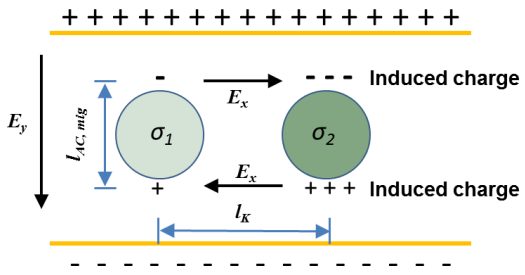

Fig. 5 Schematic of the generation of E_x due to induced charge caused by electric migration of ions under E_y. σ_1 and σ_2 indicates different σ structures. Under E_y, different number of ions are induced because of the different σ. The ions subsequently cause E_x in *x*-direction.

Based on the analysis above, E_x and E_z can be confidently neglected and the 1D electric field approximation is reasonable.

From the aforementioned 1D approximation, we derived the scaling exponents from *v*-component (*y*-directional velocity). The scaling law is also applicable for the *u*- and *w*-components. As shown in FIG. 4(b), due to **H1.1** and **H1.2**, at the scales larger than l_K, the vortex turnover time of velocity structures induced by EBF can be estimated by $l_K / \sqrt{S_v^2(l_K)}$. This is still smaller than the time request for the kinetic energy to be dissipated, i.e. l_K^2/ν. Hence, there is sufficient time for the EBF induced velocity structure to roll-up into vortex by the nonlinear inertia terms of Eq. (5). An approximately isotropic 3D velocity field is predictable.

5.4 The validity of H3

As have been introduced in section 2.1, this hypothesis is based on the experimental observation of Wang et al. [16, 18]. In the investigation, they applied a 100 kHz AC electric field to disturb the originally laminar flow to generated turbulent-like flow. However, in the velocity spectrum, even if the temporal resolution of their velocity measurement method is sufficiently high, there is no any peak at the forcing frequency, i.e. 100 kHz. The velocity responds at much lower frequency regions (below 2 kHz). This indicates there is no direct energy injection at 100 kHz and the inverse cascade is not present. Meanwhile, the instant AC electric field has no straightforward interaction with the velocity field and the corresponding conductivity field. This phenomenon has never been found in all the known turbulent models. However, this phenomenon is not rare in AC EK flows, as have been discussed by Ramos et al. [21]. From the phenomenon above, we made the **H3** hypothesis, which is reasonable and observable.

5.5 Discussion on the Weak EK turbulence

In weak EK turbulence, because of the different scaling

exponents between EBF and buoyance, the inertial subrange in EK turbulence is predicted to be on the lower wavenumber side of the EBF dominant region, while in the RB turbulent convection, BO59 scaling region is on the higher wavenumber side of the inertial subrange. However, similar to the latter one, where the co-existence of BO59 scaling region and inertial subregion is questionable [9], the co-existence of EBF dominant region and inertial subregion can only be confirmed by experimental investigations in future. Since in the case, the inertial subrange is pre-required for conductivity to cascade to small scales, the co-existence of EBF dominant region and inertial subrange is more practical in macroscale hydrodynamic turbulence.

5.6 Possible ways of generating and measuring the EBF dominated subrange

As have been shown in Eq. (57) and (63), to realize EBF dominated subrange, one should decrease l_{ek}/l_0 or l_K/l_0. This can be achieved by several ways: (1) Decrease $\langle|\theta_{l_0}|\rangle$. However, to sustain σ cascade, $\langle|\Delta\sigma(l_0)|\rangle$ should be sufficiently large. Therefore, $\langle\sigma\rangle_w$ must be large enough to reach small $\langle|\theta_{l_0}|\rangle$, i.e. high conductivity fluids are preferred. (2) Use small β_w. Note, although small $\beta_w$is preferred, it cannot be too small. Otherwise, electrolysis may happen. (3) Use strong enough electric field intensity. (4) Apply low viscosity fluids. (5) Use a channel or vessel with a large dimension, i.e. large l_0. The condition (5) indicates, if the electric field intensity can be sufficiently high, the EBF dominated subrange is more observable in macroflow rather than microflow.

In fact, by applying a strong DC electric field on two immiscible fluids (but still has multiscale structures), Varshney et al (2016) [36] observed a turbulent like flow with a slope of -1.4 in the velocity power spectrum. This is exactly what we predicted here. The experimental observation of Varshney et al (2016) indicates the present theory can be applied not only to single phase flows, but also multiphase flows where dispersed phases have a different conductivity from the continuous phase. Although the experiments were carried out in a DC case, physically say, the DC case could be considered as an asymptotic result when the frequency of AC approaches zero. They have similar scaling behaviors. This is out of the scope of the current work and will be discussed in detail in the future. We believe, if the channel used in Wang et al. [18] is enlarged, the scaling law predicted in this manuscript could also be realized.

To validate the present theory of the AC EK turbulence experimentally, no matter in macro- or microflows, simultaneously ultrahigh spatial and temporal velocimeter is required. For the velocity measurement, unfortunately, current standard velocimeters, such as Particle Imaging Velocimetry and Laser Doppler Velocimetry, have difficulties to measure the unsteady velocity fluctuations with high frequency in the EK turbulence, as explained by Zhao et al (2016)[37]. For instance, in unsteady EK flows, velocity of particle should be different from their surrounding fluids, due to not only electrostatic force (particles are normally not electrically neutral), but also particle lagging, dielectrophoresis, electrothermal flows and etc. Recently developed Laser Induced Fluorescence Photobleaching Anemometer (LIFPA)[16] which using uniform fluorescent dyes may provide us a new opportunity to measure the EK turbulence with simultaneously ultrahigh spatial and temporal resolutions.

For the conductivity measurement, to the best of authors' knowledge, there is no non-invasive method can directly measure conductivity fluctuations with both high spatial and temporal resolutions. The most commonly used non-invasive conductivity measurement method is Electrical Impedance Tomography [38]. However, the capturing rate of images is only tens of frames/second and the spatial resolution is on the order of millimeter. Such a capturing rate and spatial resolution is far from the requirement of measuring conductivity fluctuations, which can be more than 1 kHz in frequency and smaller than 1 μm in length. Besides, under the external electric field, Electrical Impedance Tomography is unable to provide reliable measurement.

6. Conclusion

In this manuscript, the cascade process of kinetic energy in the AC EK turbulence with high frequency is theoretically investigated. Similar as the buoyancy controlled subrange predicted by BO59 law, the EBF dominated subrange is theoretically studied. Coupled with the direct cascade process of conductivity, it is found the energy cascade in the EBF dominated subrange is neither a purely direct process, nor a purely inverse process. The high frequency AC electric field and the corresponding EBF do not drive the flow directly, but indirectly through electric conductivity structures in a much lower frequency range. In the EBF dominated subrange, we theoretically find the scaling exponents of the 2nd order velocity and conductivity structural functions are 2/5 and 4/5 respectively. Compared to the buoyancy in thermal convections, EBF is more effective and sustainable at small scales. Based on the EBF strength, two cascade processes are predicted, i.e. the Weak EK turbulence and Strong EK turbulence. Correspondingly, two characteristic small length scales, l_{ek} (analogous to Bolgiano scale in thermal convection) and l_K, are also predicted.

EK turbulence is a new interdisciplinary phenomenon and far from understanding. The present study theoretically reveals the characters and mechanisms of the AC EK turbulence. It covers broad interests between conventional turbulence in physics and lab-on-a-chip where EK mechanisms are frequently used to manipulate flows. From the investigation of scaling behaviors of both the EBF and the velocity structure, we find that EK forcing is an effective way

to control flow and generate turbulence, and hence, enhance mixing in both micro- and macroflows. It can significantly augment cascade process from large to small scale for both momentum and scalar. The EK turbulence theory is not restricted in a single phase fluid, but also multiphase fluids and any mixture in fluids with different electric characteristics. This will help us understand the fluid behavior in complex circumstances, where electric field is present. Furthermore, the investigations on forced turbulence and its forced cascade region can significantly deepen our understanding on the interactions between external force and turbulent flow. This will open a door to flexibly manipulate and control the cascade process of flows in future.

7. Acknowledgement

The work was supported by NSF grant no. CAREER CBET-0954977, MRI CBET-1040227 and CBET-1336004, respectively.

Reference

1. Kolmogorov, A.N., *The Local Structure of Turbulence in Incompressible Viscous Fluid for Very Large Reynolds Numbers.* Dokl. Akad. Nauk SSSR, 1941. **30**(4).
2. Davidson, P.A., *Turbulence - An Introduction for Scientists and Engineers*. 2004, New York: Oxford Univesity Press.
3. Obukhov, A.M., *Structure of the temperature field in turbulent flow.* Izv. Akad. Nauk. SSSR, Ser. Geogr. and Geophys, 1949. **13**(1): p. 58-67.
4. Corrsin, S., *On the Spectrum of Isotropic Temperature Fluctuations in an Isotropic Turbulence.* Journal of Applied Physics, 1951. **22**(4): p. 469-473.
5. Batchelor, G.K., *Small-scale variation of convected quantities like temperature in turbulent fluid. Part 1. General discussion and the case of small conductivity.* Journal of Fluid Mechanics, 1959: p. 113-133.
6. Bolgiano, R., *Turbulent spectra in a stably stratified atmosphere.* Journal of Geophysical Research, 1959. **64**(12): p. 2226-2229.
7. Obukhov, A.M., *On the influence of Archimedean forces on the structure of the temperature field in a turbulent flow.* Dokl. Akad. Nauk. SSR, 1959. **125**: p. 1246-1248.
8. Niemela, J.J., et al., *Turbulent convection at very high Rayleigh numbers.* Nature, 2000. **404**: p. 837-840.
9. Lohse, D. and K.-Q. Xia, *Small-Scale Properties of Turbulent Rayleigh-Bénard Convection.* Annual Review of Fluid Mechanics, 2010. **42**: p. 335-364.
10. Chertkov, M., *Phenomenology of Rayleigh-Taylor Turbulence.* Physical Review Letter, 2003. **91**(11): p. 115001.
11. Boffetta, G., et al., *Bolgiano scale in confined Rayleigh–Taylor turbulence.* Journal of Fluid Mechanics, 2012. **690**: p. 426–440.
12. Zhou, Q., *Temporal evolution and scaling of mixing in two-dimensional Rayleigh-Taylor turbulence.* Physics of Fluids, 2013. **25**: p. 085107.
13. Saville, D.A., *Electrokinetic effects with small particles.* Annual Review of Fluid Mechanics, 1977. **9**: p. 321-337.
14. Davidson, J.H. and E.J. Shaughnessy, *Turbulence generation by electric body force.* Experiments in Fluids, 1986. **4**: p. 17-26.
15. Kourmatzis, A. and J.S. Shrimpton, *Turbulent three-dimensional dielectric electrohydrodynamic convection between two plates.* Journal of Fluid Mechanics, 2012. **696**: p. 228-262.
16. Wang, G., F. Yang, and W. Zhao, *There can be turbulence in microfluidics at low Reynolds number.* Lab on a Chip, 2014. **14**(8): p. 1452 - 1458.
17. Wang, G., et al., *On micro-electrokinetic scalar turbulence in microfluidics at low Reynolds number.* Lab on a Chip, 2016. **16**: p. 1030-1038.
18. Wang, G., F. Yang, and W. Zhao, *Micro electrokinetic turbulence in microfluidics at low Reynolds number.* Physical Review E, 2016. **93**(013106).
19. Grossmann, S. and V.S. L'vov, *Crossover of spectral scaling in thermal turbulence.* Physical Review E, 1993. **47**(6): p. 4161-4168.
20. Baygents, J.C. and F. Baldessari, *Electrohydrodynamic instability in a thin fluid layer with an electrical conductivity gradient.* Physics of fluids, 1998. **10**(1): p. 301-311.
21. Ramos, A., et al., *AC electrokinetics: a review of forces in microelectrode structures.* Journal of Physics D: Applied Physics, 1998. **31**: p. 2338-2353.
22. Melcher, J.R., *Continuum Electromechanics*. 1981, Cambridge, MA: MIT Press.
23. Fouxon, A. and V. Lebedev, *Spectra of turbulence in dilute polymer solutions.* Physics of Fluids (1994-present), 2003. **15**(7): p. 2060-2072.
24. Lide, D.R., *CRC Handbook of Chemistry and Physics, 90th Edition*. 90th ed, ed. D.R. Lide. 2009, Boca Raton, FL: CRC Press/Taylor and Francis.
25. Rienstra, S.W. and A. Hirschberg, *An Introduction to Acoustics*. 2004, Eindhoven University of Technology.
26. Campisi, M., et al., *A soft-lithographed chaotic electrokinetic micromixer for efficient chemical reactions in lab-on-chips.* Journal of Micro-Nano Mechatronics, 2009. **5**: p. 69-76.
27. Chen, C.-H., et al., *Convective and absolute electrokinetic instability with conductivity gradients.* Journal of Fluid Mechanics, 2005. **524**: p. 263-303.
28. Chen, C.o.-K. and C.-C. Cho, *Electrokinetically driven flow mixing utilizing chaotic electric fields.* Microfluidics and Nanofluidics 2008. **5**(6): p. 785-793.
29. Lee, Y.-K., et al., *Chaotic mixing in electrokinetically and pressure driven micro flows*, in *MEMS 2001. 14th IEEE International Conference on Micro Electro Mechanical Systems.* 2001: Interlaken, Switzerland. p. 483-486.
30. Park, J., et al., *Application of electrokinetic instability for enhanced mixing in various micro–T-channel geometries.* Physics of Fluids, 2005. **17**: p. 118101.
31. Saddoughi, S.G. and S.V. Veeravalli, *Local isotropy in turbulent boundary layers at high Reynolds number.* Journal of Fluid Mechanics, 1994. **268**: p. 333-372.
32. Sreenivasan, K.R., *On local isotropy of passive scalars in turbulent shear flows.* Proc. R. Soc. Lond. A, 1991. **434**: p. 165-182.
33. Warhaft, Z., *Passive scalars in turbulent flows.* Annu. Rev. Fluid Mech. , 2000. **32**: p. 203-240.
34. Lee, C.-Y., et al., *Microfluidic Mixing: A Review.* International Journal of Molecular Sciences, 2011. **12**: p. 3263-3287.
35. Edward, P.L., V.A. Atiemo-Obeng, and S.M. Kresta, *Handbook of*

Industrial Mixing: Science and Practice. 2004: John Wiley & Sons.

36. Varshney, A., et al., *Multiscale flow in an electro-hydrodynamically driven oil-in-oil emulsion.* Soft Matter, 2016. **12**: p. 1759-1764.
37. Zhao, W., et al., *Measurement of velocity fluctuations in microfluidics with simultaneously ultrahigh spatial and temporal resolution.* Experiments in Fluids, 2016. **57**(11): p. 1-12.
38. Bayford, R.H., *Bioimpedance Tomography (Electrical Impedance Tomography).* Annual Review of Biomedical Engineering, 2006. **8**: p. 63-91.